Fundamental framework to design multiple rigid barriers for resisting debris flows

Ng, Charles W.W.[1], Choi, C.E.[2], Majeed, U.[1], Poudyal, S.[1] and De Silva, W.A.R.K.[1]

[1]Department of Civil and Environmental Engineering, Hong Kong University of Science and Technology, Hong Kong SAR
[2]Department of Civil Engineering, The University of Hong Kong, Hong Kong SAR

ABSTRACT

Hong Kong, Taiwan and numerous other areas around the world are vulnerable to debris flows. A single rigid barrier is generally installed at the end of a potential flow path to intercept such flows. However, such an approach enables flows to accelerate and increase in volume before impacting a rigid barrier. Thus, large barriers are required to resist higher impact forces. An alternative to a single rigid barrier is series of small rigid barriers installed along a potential flow path. However, no such design codes are available for engineers to design safe and economical multiple barriers. One of the major challenges in designing multiple rigid barriers is determining the appropriate spacing between the barriers to optimise the design of subsequent barriers in the flow channel. A new analytical framework developed to design multiple rigid barriers is presented in this keynote paper. The impact of a debris flow on a barrier is scale dependent; thus, the analytical framework is evaluated by three types of flows impacting dual rigid barriers in two different sized flumes. Physical experiments using dry sand in a 5 m-long flume and water and two-phase flows in a 28 m-long flume are conducted. The validity of the framework is verified and findings are discussed.

Keywords: Debris flow; dual rigid barriers; flume; impact

1. BACKGROUND

The design of multiple barrier systems to arrest debris flows is a scientific and engineering challenge for two main reasons. Firstly, debris flows impacting barriers are rarely observed in the field. Therefore, the fundamental mechanisms of impact have yet to be elucidated. The adequacy or overdesign of a barrier cannot be ascertained until such fundamental mechanisms are understood. Secondly, debris flows are scale-dependent phenomena (Iverson 2015). Thus, the timescale for pore pressure dissipation and degree of viscous shearing can considerably change the macroscopic flow dynamics, depending on the flow depth. Based on these considerations, unique physical modelling facilities are required to capture the appropriate dynamics to validate theories and enhance practical designs.

A commonly adopted approach for intercepting debris flows is the construction of a single rigid barrier (Lo 2000) at the end of a catchment (Fig. 1). However, such an approach enables flows to increase in speed and volume (Berger et al. 2011) before impacting the barrier. Consequently, a large barrier with a high resisting capacity is required. To address this challenge, several small rigid barriers along a flow path can be used to progressively dissipate the energy of a debris flow and reduce its overall volume. Although the use of multiple rigid barriers is a promising solution, scientific-based guidelines to optimise their design have yet to become available. The interaction between debris flow and multiple rigid barriers is governed by the overflow trajectory and the energy dissipated upon landing before the debris flow impacts the subsequent barrier in the channel. Therefore, a fundamental understanding of overflow and landing (Kwan et al. 2015) mechanisms between barriers is essential to achieve an optimised design.

Fig. 1. Rigid barrier to resist debris flow

In international design guidelines (Kwan 2012; Volkwein 2014), the dynamic impact force exerted by a debris flow is generally based on the conservation of linear momentum, which is given as follows:

$$F = \alpha \rho v^2 h_0 w \quad (1)$$

where α is an impact coefficient; ρ is the flow density; v is the velocity of the flow; h_0 is the flow depth and w is the channel width. If α is unity, then the impact scenario is inelastic. However, if α is two, then the impact scenario is elastic. To ensure robust barrier designs, international guidelines (Lo 2000; ASI 2008) often prescribe high α values to account for the idiosyncrasies involved in natural materials and settings in the field. For example, Kwan (2012) recommends an α of 2.5 for the design of rigid reinforced concrete barriers. Although existing guidelines may provide a conservative estimate of the impact load on a single barrier, the effects of the first barrier on the velocity of the flow before impacting the subsequent barrier are not explicitly considered.

An analytical framework developed to design multiple rigid barriers is presented in this keynote paper. The framework is evaluated by physical experiments for three types of flows, namely, dry sand, two-phase debris and water flows. Dual rigid barriers are investigated in these experiments.

2. FRAMEWORK TO DESIGN MULTIPLE RIGID BARRIERS

Fig. 2 illustrates the multiple rigid barrier framework reported by Kwan et al. (2015) and Ng et al. (2018). The framework includes a velocity attenuation impact model that captures the dissipation of kinetic energy as granular material is deposited in layers up to the crest of a barrier (Choi et al. 2015a). The overflow follows the trajectory of an inviscid jet after the flow reaches the crest of the barrier and lands on the channel bed. The overflow trajectory is dependent on the height of the barrier and on the overflow velocity. The trajectory can be used to determine the appropriate spacing between barriers. The energy that dissipates when the overflow lands on the channel is dependent on the impact angle. The velocity of the flow before impacting the subsequent barrier in the channel can then be determined. The aforementioned mechanisms occur iteratively in the entire multiple barrier system. Several details of the framework are briefly presented below.

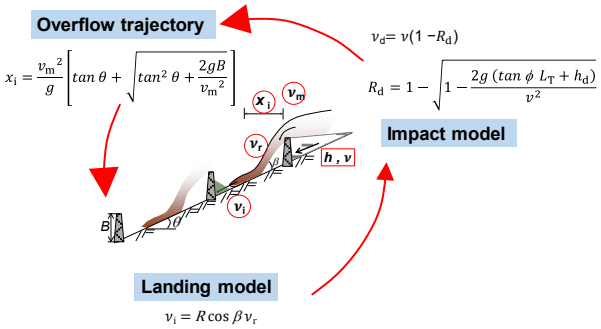

Fig. 2. Multiple barrier framework (Kwan et al. 2015; Ng et al. 2018)

2.1 Velocity attenuation impact model

Granular material is arrested when dry granular flow impacts a rigid barrier. Henceforth, the arrested material is referred to as the dead zone. Sand piles on top of the dead zone in layers up to the crest of the barrier as an increased amount of sand impacts the barrier (Koo et al. 2017). Fig. 3 shows a granular flow with velocity v and depth h_0 on an incline θ. The flow climbs on a wedge of arrested material, and the kinetic energy of the flow is attenuated via the drag between the arrested and the flowing material. The run-up velocity v_d and the velocity attenuation factor R_d can be calculated according to Newtonian mechanics. The attenuation is described as follows:

$$v_d = v\,(1 - R_d) \quad (2)$$

$$R_d = 1 - \sqrt{1 - \frac{2g\,(\tan\phi\, L_T + h_d)}{v^2}} \quad (3)$$

where g is the acceleration due to Earth's gravity, ϕ is the angle of repose, L_T is the length of the free surface of the arrested granular material and h_d is the height of the deposited granular material. Eqns. 2 and 3 are used iteratively until the granular material has reached the crest of the barrier.

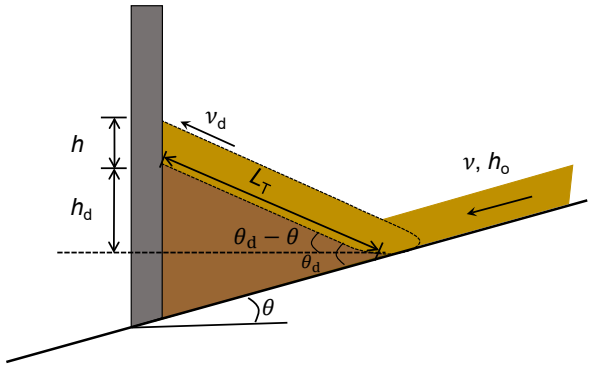

Fig. 3. Schematic diagram showing the layering mechanism in the velocity attenuation model proposed by Koo et al. (2017)

2.2 Overflow trajectory

Overflow occurs when granular material reaches the crest of a barrier. The overflow trajectory in the proposed framework assumes that the granular jet launches horizontally from the crest (Kwan et al. 2015). The trajectory is estimated based on the kinetic equations of motion by assuming that the overflow is a point mass. The horizontal overflow distance before the flow lands on the channel x_i is given as follows:

$$x_i = \frac{v_m^2}{g}\left[\tan\theta + \sqrt{\tan^2\theta + \frac{2gB}{v_m^2}}\right] \quad (4)$$

where v_m is the horizontal overflow velocity and B is the barrier height. The horizontal distance required to land on the channel can then be used to determine the appropriate spacing between the barriers. Specifically, the spacing between barriers must be larger than x_i so overflow does not launch over the subsequent barrier in the channel. Ideally, the overflow should be allowed to impact the channel bed before it is allowed to impact the subsequent barrier in the channel to maximise the energy dissipated in the flow.

2.3 Landing

Energy is attenuated when the overflow lands on the channel. Therefore, the velocity of the flow before reaching the subsequent barrier v_i depends on the slope-parallel component of the landing velocity v_r and the landing angle β at which the flow impacts the channel bed. The ratio of velocity after and before landing is referred to as the landing factor Cr, which accounts for momentum loss upon landing. The Cr is given as follows:

$$Cr = R\cos\beta \quad (5)$$

where R is the coefficient accounting for the energy loss due to friction between the flow and channel bed upon landing.

3. PHYSICAL MODELLING OF DRY SAND FLOWS

A 5 m-long rectangular flume is used to examine the impact dynamics of dry sand flows impacting dual rigid barriers (Choi et al. 2014, 2016b, 2018). The channel has a depth of 500 mm and a width of 200 mm. A hopper with a maximum volume of 0.06 m^3 holds the granular material, which is retained behind a remote-controlled gate.

3.1 Instrumentation

Fig. 4 shows a side view of the 5 m-long flume and the instrumentation layout. Flow kinematics are captured by using high-speed cameras at the side of the channel. These cameras capture images at a resolution of 1,300 × 1,600 pixels and a rate of 640 frames per second. Images are analysed using particle image velocimetry (White et al. 2003). Laser displacement sensors are used to measure the flow depth directly upstream of both barriers along the centreline of the channel.

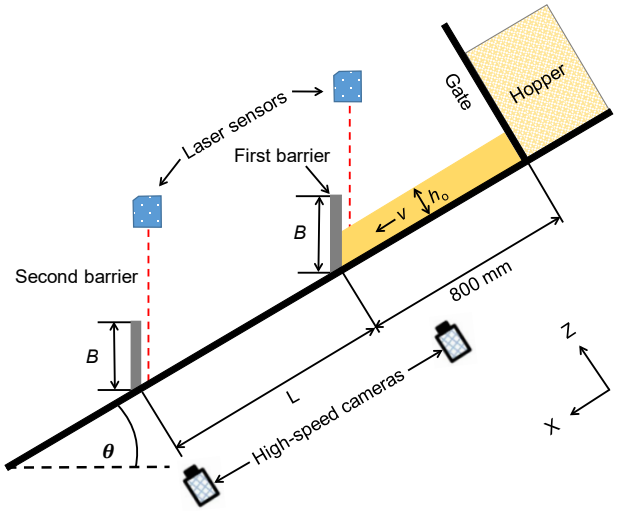

Fig. 4. Side view of 5 m-long flume model setup

3.2 Test programme

Open-channel tests are carried out to characterise the Froude number Fr of the flows for each test. The inclination in each open-channel test is set as 26° to develop flows with a preimpact Fr of about 4, which is typically observed in the field (Hübl et al. 2009; Kwan 2012). Previous studies (Faug et al. 2003, 2004, 2008a; Faug 2015; Hákonardóttir et al. 2003; Choi et al. 2015b) have indicated that the ratio between the flow depth and the barrier height governs the prevailing impact and overflow mechanisms; thus, three ratios are investigated (refer to Table 1). The measured maximum flow depth h_0 in the open-channel tests is 90 mm. Table 1 summarises the test programme.

Table 1. Tests programme for 5 m-long flume tests

Test ID	First barrier height B (mm)	Normalised barrier height B/h_o
FF	-	-
B260	260	2.9

B180	180	2.0
B100	100	1.1

Note: Constant barrier spacing L of 700 mm

3.3 Testing procedures

Dry Leighton Buzzard fraction C sand with a mean particle diameter D_{50} of 0.6 mm is used for 5 m-long flume experiments. The sand has an angle of repose of 30° and an interface friction angle of 22.6° with the channel bed, which is determined by the tilt test reported by Pudasaini and Hutter (2007). Dry sand with a total mass of 100 kg is placed in the hopper with a target bulk density of approximately 1,680 kg/m^3 for each 5 m-long flume test in this study. The flume is inclined to 26° before the gate is opened to simulate dam-break (Choi et al. 2014).

4. PHYSICAL MODELLING OF TWO-PHASE AND WATER FLOWS

A large flume model is necessary to examine the impact mechanisms of viscous two-phase flows to ensure that the timescale for pore pressure dissipation in the flow and the contribution of viscous shearing relative to the flow inertia are similar to those observed in the field. A unique 28 m-long flume (Fig. 5) is used to model the debris flow impacting dual rigid barriers. The channel has a width and a depth of 2 m and 1 m, respectively. A hopper that can hold up to 10 m^3 of debris occupies the first 5 m of the channel, which is inclined at 30°. The second part of the channel is 15 m in length and inclined at 20°. The third part of the channel is horizontal and 8 m long. A double gate system is used to retain debris material inside the hopper. The gates are secured by a mechanical arm that is controlled by an electric motor.

4.1 Instrumentation

Newly developed instrumentation cells (Fig. 6) are installed at regular intervals of 5 m along the base of the channel. Each cell measures normal and shear stresses induced by the flow by using the triaxial load cells. The load cell is mounted on the steel frame which is secured on the flume base by using screws. Moreover, changes in pore water pressure at the base of the flow are measured by pore pressure transducers. Pore pressure transducer is connected at the bottom of the pore pressure adapter. The top part of pore pressure adapter has a steel mesh with an opening size of ~1.5 mm to prevent coarse particles entering the adapter. The adapter is a cylindrical box with inner height and radius of 30 mm and 20 mm, respectively. It is filled with water prior to the test so the pore pressure can be recorded instantaneously when flow passes over the instrumentation cell. Laser and ultrasonic displacement sensors are mounted above each instrumentation cell to measure the flow depth along the centreline of the channel. The flow depth and normal stress are used to approximate the bulk density of the flow. However, we only report the pore pressure data in this keynote paper, whilst a detailed analysis of normal stress will be given by Majeed (2020). Furthermore, the same high-speed camera that is used in the 5 m-long flume tests is used in the 28 m-long flume tests. Additionally, a video camera mounted onto a drone is used to capture an aerial view of the experiment. Compression load cells for dynamic loading are installed behind each rigid barrier model to measure the total impact force. Details of the model barriers for the 28 m-long flume experiments are discussed below. All measurements are sampled at a rate of 2 kHz.

4.2 Test programme and procedure

Fig. 7 shows a texture classification of debris flow mixtures consisting of different percentages of gravel, sand and fines (silt and clay). A comparison is conducted between field mapping data from 50 debris flow events that occurred in June 2008 in Hong Kong (Sze and Lam 2017), relevant experiments (Bugnion et al. 2012; Iverson et al. 2010) and natural debris flows (Takahashi et al. 1991; Remaitre et al. 2003; Chou et al. 2007; Tecca et al. 2007). The majority of the debris flows shown are predominantly sand–gravel mixtures, with limited samples of clay-rich debris. Mixtures with fine contents greater than 20% are classified as muddy flows (Bonnet-Staub 1999). Viscous stresses dominate the flow dynamics of such flows, whereas grain and fluid viscous stresses dominate the macroscopic flow dynamics of granular flows (fines < 20%) (Iverson 1997). Evidence of site-specific geomorphology on debris mixtures can be seen in the texture classification. Debris flows from Hong Kong, Korea and Taiwan are granular and generally contain a low percentage of fines (<10%). A debris mixture representative of East Asia is selected for this study, which comprises 35% gravel (20 mm), 62.5% sand (0.6 mm), and 2.5% clay (< 2 μm). A volume of 2.5 m^3 of debris material with a 0.6 solid fraction is prepared for each test. A solid fraction of 0.6 is typical in field debris flows (Iverson 2015). The initial density of the mix is approximately 2,000 kg/m^3. This density lies within the range observed for natural debris flows, which typically ranges from 1,700 kg/m^3 to 2,400 kg/m^3 (Iverson and George 2014). The debris material is prepared in a concrete mixer to achieve uniform mixing. The uniformly mixed material is then placed into the storage container. Similarly, a volume of 2.5 m^3 is used for the water test.

The first rigid barrier is constructed for the dual rigid barrier test by using an aluminium plate (Fig. 8) with a height of 500 mm and a width of 2,000 mm. Two rigid supports are installed on the sides of the channel to hold the aluminium plate in place. A load

cell is sandwiched between the plate and the rigid supports to measure the impact force. The second rigid barrier comprises a steel plate mounted on a reinforced concrete structure. The steel plate is 1,500 mm high and 2,000 mm wide. Load cells are installed at each corner behind the steel plate. The first rigid barrier is installed at an inclined distance of 11 m from the gate, and the second rigid barrier is installed at a curvilinear distance of 6 m from the first barrier. The spacing between the barriers is determined by Eqn. 4, which ensures that the overflow lands between the barriers. The flow is initiated after the instrumentation is prepared by opening the gate.

Fig. 5. Plan view of the 28 m-long flume model

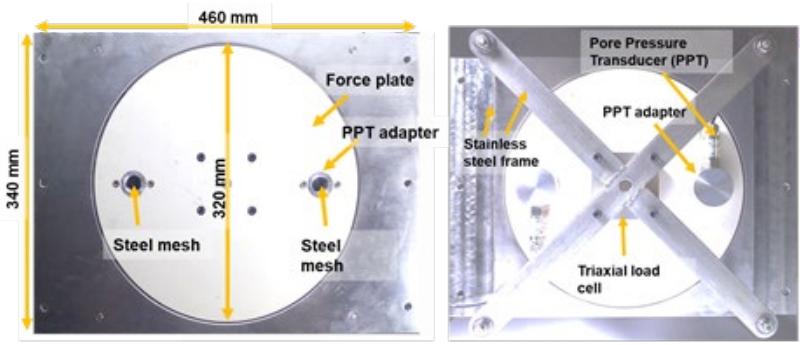

Fig. 6. Instrumentation cell: (a) top view; (b) bottom view

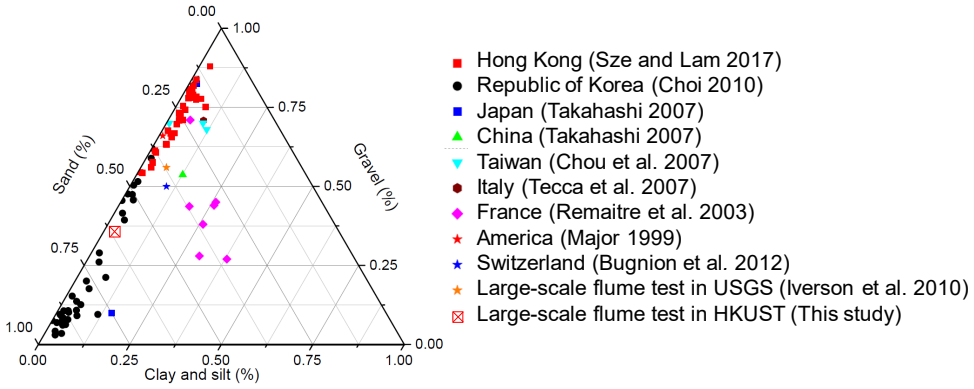

Fig. 7. Debris flow composition

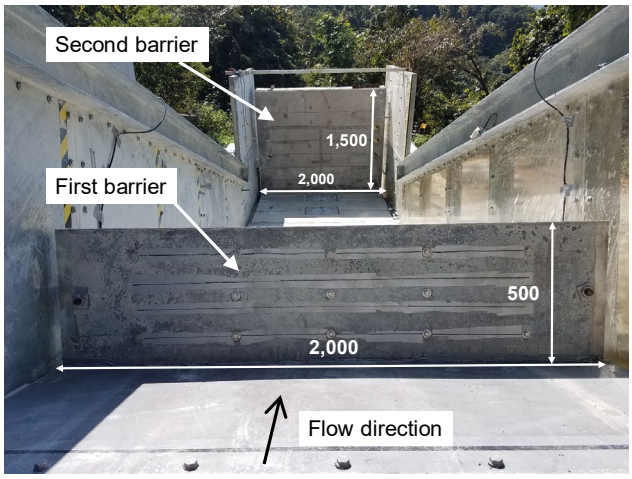

Fig. 8. Model dual rigid barriers; all dimensions are in mm

5. EVALUATION OF MULTIPLE BARRIER FRAMEWORK

This section evaluates the aforementioned multiple barrier framework (Eqns. 2 to 5) for dry sand, water and two-phase debris flows impacting dual rigid barriers.

5.1 Run-up velocity

Fig. 9 compares the measured and calculated values of the velocity attenuation impact model (Eqn. 2) for dry sand, water and two-phase debris flows impacting a rigid barrier. The dry sand flows are modelled in the 5 m-long flume, whilst the water and two-phase flows are modelled in the 28 m-long flume. The calculated velocity of the flow as it runs up along the barrier is compared with the measured velocity to evaluate Eqn. 2. The initial flow velocity measured in the physical 5 m-long flume is used to calculate the velocity attenuation by using Eqn. 2. Therefore, the measured and calculated velocities at the base of the barrier are initially the same. The run-up velocity v_d is normalised by the flow velocity v before impacting the rigid barrier, whereas the run-up height h_d is normalised by the maximum flow depth h_o. The results from the dry sand tests show that velocity is attenuated as the flow is deposited in layers up to the barrier crest. The calculated velocities agree well with the measured velocities.

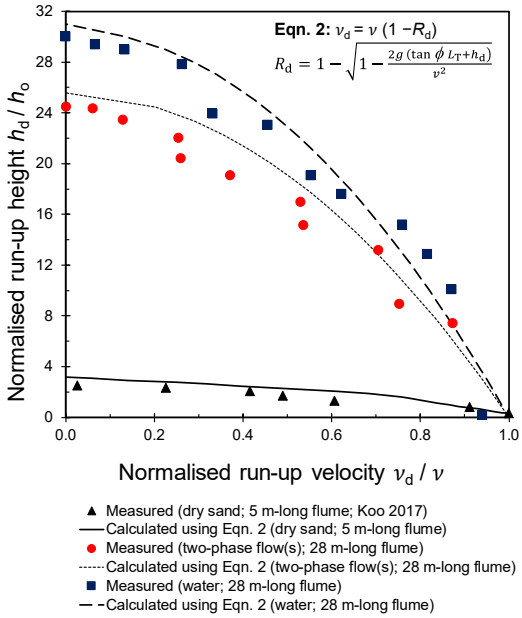

Fig. 9. Comparison of measured and calculated run-up velocity with barrier height

Similarly, the results of the water and two-phase debris flows from the 28 m-long flume tests show a reasonable agreement with the calculated values.

Fig. 10 shows the time history of the measured pore pressure, the flow depth and the calculated hydrostatic pore pressure for the two-phase debris flow. Pore pressure is measured by a pore pressure transducer installed in the instrumentation cell. The flow depth is obtained from the ultrasonic sensor installed above the instrumentation cell. The hydrostatic pressure is calculated as $p_h = \rho_f g h \cos\theta$, where p_h is the hydrostatic pore pressure, ρ_f is the fluid density taken 1,000 kg/m^3 and h is the measured flow depth from the ultrasonic sensor. The measured flow depth increases to a peak value of 90 mm and then decreases to 5 mm corresponding to the depth of debris deposited on the channel after the

test. Similarly, pore pressure measurements increase to a peak value and then decrease to zero at the end of the test, which is expected. However, a delay of approximately 1 second is observed in the maximum measured pore water pressure compared with the flow depth measurements. The delay may be because the flow front consists of a high fraction of gravel due to the particle size segregation (Iverson et al. 2010). Such a gravelly flow front has high water permeability, compared with the rest of the flow. The high permeability enables the induced excess pore pressure over the hydrostatic pore pressure to dissipate quickly. Pore pressure increases to 2.4 kPa as the flow front passes the instrumentation cell. The measured pore pressure exceeds the hydrostatic pore pressure by up to 3 times the hydrostatic pressure after 1.7 seconds. Finally, pore pressure starts to decrease as the flow tail passes but remains in excess of the hydrostatic pressure in the flow tail for approximately 7 seconds.

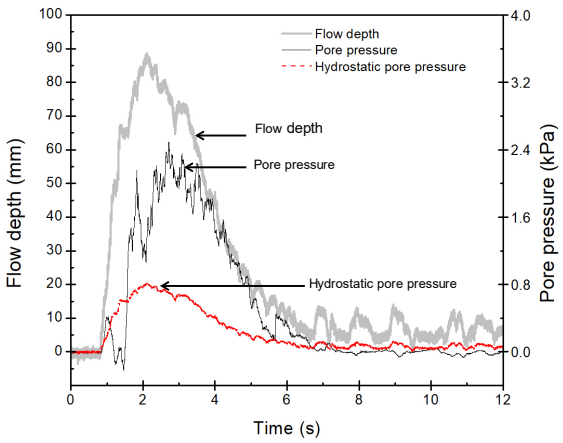

Fig. 10. Measured flow depth, basal pore pressure and total stress of the two-phase flow in the 28 m-long flume (instrumentation cell 2)

It is reasonable to deduce that the debris flow is fluidised (Iverson and Denlinger 2001) by estimating the normal stress of the flow acting on the flume bed from the measured flow depth and excess pore pressure in flow body over the calculated hydrostatic pore pressure. This deduction means that the grains in the flow are suspended and are unlikely to dissipate energy via shearing among the grains. A mobilised friction angle ϕ_m of zero is used for two-phase flows based on the measured pore water pressure to calculate the attenuated velocities using Eqn. 2. On the contrary, dry sand flow is frictional with sustained grain contacts. The mobilised friction angle for dry sand is assumed to be equal to 30° in Eqn. 2 for simplicity. A comparison between dry sand and two-phase debris flow shows that two-phase debris flow reaches a much higher run-up height owing to their fluidised state and reduced grain contacts (Fig. 9). Similarly, water flows exhibit an even higher run-up height compared with that of two-phase debris flow because water has a lower dynamic viscosity than the clay–water mixture in debris flow. A low dynamic viscosity results in less energy dissipation via viscous shearing. A comparison of measured and calculated velocities for the three different types of flows reveals that Eqn. 2 can capture velocity attenuation for a wide range of geophysical flows—from frictional dry sand flows to viscous debris and water flows.

5.2 Overflow distance

Fig. 11 compares the measured and calculated overflow distances for dry sand, water and two-phase debris flows. The calculated values are obtained by using Eqn. 4. The effects of barrier height and channel inclination on overflow distance are examined. The overflow distance x_i and barrier height B are normalised by the flow depth h_0 before the flow impacts the rigid barrier. In the tests conducted with dry sand, the normalised barrier height B/h_0 varies as 1.1, 2.0 and 2.9 for a channel inclination of 26° and as 1.0, 1.9 and 2.7 for a channel inclination of 32°. These heights correspond to typical barrier designs observed in the field. The inclination of the channel is adjusted to vary the flow inertia before impact. On the other hand, the channel inclination is fixed to be 20° for two-phase debris flow and water flow tests conducted in the 28 m-long flume. Normalised barrier heights B/h_0 of 5.5 and 5.0 are used for the two-phase debris and water flows, respectively. A comparison of measured results from the dry sand tests with different barrier heights reveals that the overflow distance decreases with barrier height. More energy attenuates from shearing among grains and the conversion of kinetic energy to potential energy as the barrier height increases. Correspondingly, tall barriers result in low overflow velocity and short overflow distance. As expected, high channel inclinations lead to more inertial flows before impact, thereby leading to long overflow distances. The comparison between measured and calculated overflow distances for dry sand shows that calculated distances using Eqn. 4 can provide

reasonable estimates and are on the conservative side.

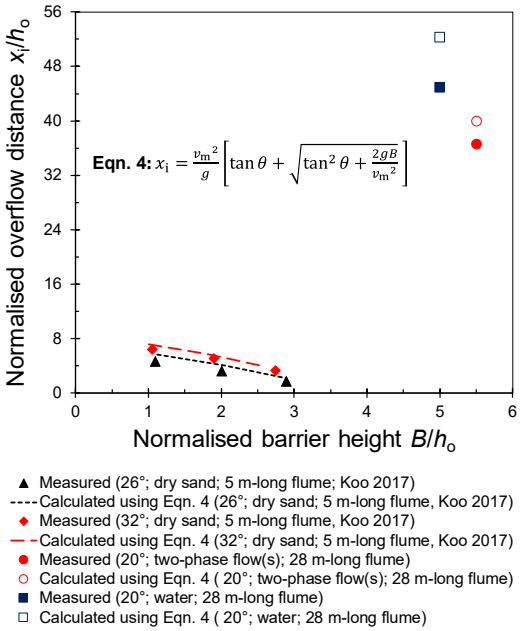

Fig. 11. Effects of channel inclination and barrier height on overflow distance

The measured overflow distances downstream from the first barrier are 4.5 m and 3.3 m for the water and two-phase debris flows, respectively (Fig. 12). The measured overflow distance for both flows is slightly lower than that calculated by using Eqn. 4, but on the conservative side. Based on the comparison of measured and calculated values, Eqn. 4 can evidently provide a reasonable estimate of the overflow distance for all three types of flows investigated in this study. Reasonable estimates of the overflow distances show that Eqn. 4 can then be used to estimate the minimum barrier spacing required between the successive barriers to ensure that the flow lands between two barriers.

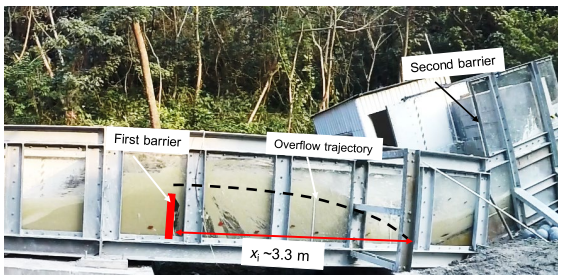

Fig. 12. Observed overflow trajectory for two-phase flow in the 28 m-long flume

5.3 Landing factor

Fig. 13 compares the estimated landing factors *Cr* using Eqn. 5 and those back calculated from the flume experiments of dry sand flows in a 5 m-long flume and two-phase debris flows in a 28 m-long flume. The back-calculated *Cr* for dry sand flows landing on the acrylic bed of the 5 m-long flume (Koo 2017) and the two-phase debris flows landing on the steel bed of the 28 m-long flume are presented. The result from the water flow is not included in the figure because the water flow was turbulent when it landed, thereby making it difficult to determine the landing velocity accurately.

The landing factor *Cr* accounts for the momentum loss from the impact between the flow and the channel bed. The measured results for the dry sand show that the landing factor *Cr* increases as the landing angle β decreases, thereby implying that less energy is dissipated upon landing. Physically, momentum is assumed to be completely destroyed when flow lands perpendicularly to the channel ($\beta = 90°$). That is, $Cr = 0$. In contrast to the perpendicular impact, no energy is dissipated from the landing ($Cr = 1$) when the flow lands tangentially ($\beta = 0°$) to the channel. A best fit line through the measured data is shown to reveal the contribution of the energy dissipated via basal friction upon landing. The projected best fit gives an *R* coefficient of 0.9 at $\beta = 0°$. This result indicates that energy dissipation from the tangential shear between the flow and the bed is only 10% of the total energy dissipated upon landing. Nonetheless, a value of $R = 1$ (no energy loss from the tangential bed shear) provides an upper bound for the dry sand and two-phase flows. The results imply that Eqn. 5 with $R = 1$ can be used to estimate the landing factor *Cr*.

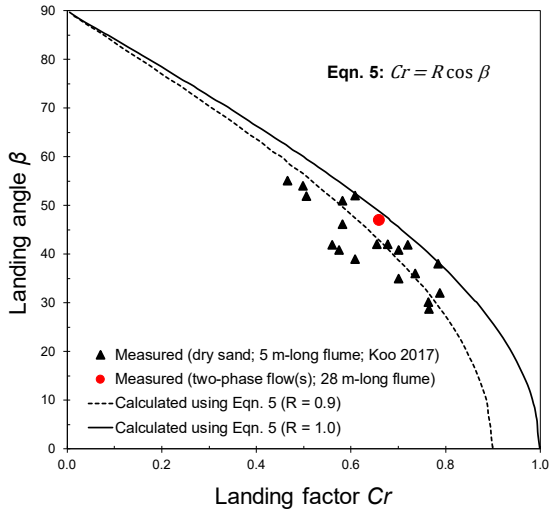

Fig. 13. Comparison of landing factor

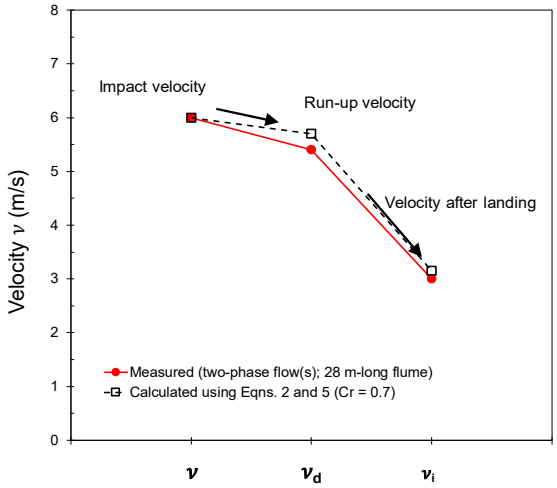

Fig. 14. Comparison of frontal velocity for dual rigid barrier system

5.4 Frontal velocities in 28 m-long flume

Three different frontal velocities for the two-phase flow are compared in Fig. 14 to evaluate the entire multiple barrier analytical framework (Eqns. 2 to 5). The calculated and measured velocities before impact, during overflow and upon landing are compared. The frontal velocity of the two-phase flow before impacting the first barrier is 6 m/s. This pre-impact velocity is adopted as the initial input for Eqns. 3 and 4. The resulting calculated overflow velocity at the crest of the barrier is 5.7 m/s, which is close to the measured velocity (5.4 m/s). Furthermore, the measured velocity after landing is 3 m/s, and the measured landing angle is 48°±2° (Cr =0.66). Notably, the water flow upon landing was turbulent, thereby making it difficult to measure the landing velocity correctly. Hence, the test result of the water flow is not included.

Velocity reduction upon landing depends on several factors, including the landing angle, the flow type and the channel bed condition. Kwan et al. (2015) reviewed field and laboratory data, including dry sand and two-phase flows impacting hard and/or soft beds. The authors reported that velocity reduction factors Cr range from 0.3 to 0.75, and recommended Cr = 0.7 for a robust design. This value considers uncertainties involved in the measurement of the landing angle and with the velocities before and after landing. The calculated post landing velocity based on the recommended Cr of 0.7 and the measured velocity are compared in Fig. 14. The calculated landing velocity is 3.2 m/s, which agrees well with the measured post-landing velocity (3 m/s) for a two-phase flow impacting a steel bed. Therefore, a Cr of 0.7 could be used to estimate the post landing velocity. In summary, the multiple barrier framework is evaluated and deemed appropriate to determine impact, overflow and landing dynamics, which are instrumental in designing multiple barrier systems.

6. KEY CONCLUSIONS

A recently developed analytical framework for multiple rigid barriers is presented in this keynote paper. The analytical framework is evaluated by physical experiments modelling dual rigid barriers impacted by dry sand flow in a 5 m-long flume, and water and viscous two-phase debris flows in a 28 m-long flume. The findings from this study can be drawn as follows.

a) In general, the newly proposed multiple barrier framework can estimate velocity attenuation during impact, overflow velocity and landing distance, for dual rigid barriers reasonably well. This framework is verified by comparing the physical model tests at two different scales (5 m and 28 m flumes) and three types of flows (dry sand, water and two-phase debris flows).
b) The overflow distance model can conservatively estimate the overflow distance for the three types of flows studied. The minimum barrier spacing should be larger than the calculated overflow distance to ensure a robust multiple barrier design.

c) Based on the experimental data from dry sand and two-phase debris flow, a landing factor of Cr = 0.7 gives a conservative estimate of flow velocity before the second barrier. The estimated velocity serves as the initial input velocity for the design of the subsequent barrier along a potential flow path.

7. LOOKING AHEAD

Debris flow modelling is a scale-dependent problem. Thus, the development and construction of the largest possible testing facilities will be necessary to advance the current state of scientific and engineering understanding on the utilisation and design of barriers to mitigate large volumes of debris flows. One of the world's largest flume is currently under construction. This facility is jointly developed by Hong Kong University of Science and Technology and the Institute of Mountain Hazards and Environment of the Chinese Academy of Sciences. The flume facility is 172 m-long with a channel width of 6 m (Fig. 15). The hopper at the most upstream end of the slope can store a debris volume of 500 m^3. This facility will be used not only to evaluate the proposed multiple barrier framework in this study but also to serve the local and international scientific and engineering community at large for decades to come.

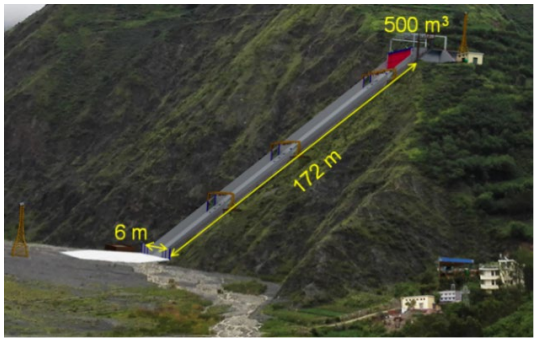

Fig. 15. Schematic of 172 m-long flume in Kunming, China

ACKNOWLEDGEMENTS

The work described in this paper was supported by two grants from the Research Grant Council of the Government of Hong Kong Special Administrative Region, China (T22-603/15-N and AoE/E-603/18). The authors would also like to thank the constructive comments on the paper provided by Dr J. S. H. Kwan and Dr R. C. H. Koo from the Geotechnical Engineering Office, Civil Engineering and Development Department, Government of the Hong Kong Special Administrative Region, China.

REFERENCES

ASI (2008). ONR 24801 Protection Works for Torrent Control - Actions on Structures (Draft). Austrian Standard Institute, Austria, 25.

Berger, C., McArdell, B. W. and Schlunegger, F. (2011). Direct measurement of channel erosion by debris flows, Illgraben, Switzerland. *Journal of Geophysical Research, Earth Surface* 116(F1).

Bonnet-Staub, I. (1999). Définition d'une typologie des dépôts de laves torrentielles et identification de critères granulométriques et géotechniques concernant les zones sources. *Bulletin of Engineering Geology and the Environment* **57**, No.4, 359–367.

Bugnion, L., McArdell, B. W., Bartelt, P. and Wendeler, C. (2012). Measurements of hillslope debris flow impact pressure on obstacles. *Landslides* **9**, No. 2, 179–187.

Choi, C. E., Ng, C. W. W., Song, D., Kwan, J. S. H., Shiu, H. Y. K., Ho, K. K. S. and Koo, R. C. H. (2014). Flume investigation of landslide debris-resisting baffles *Canadian Geotechnical Journal* **51**, No. 5, 540–553.

Choi, C. E., Au-Yeung, S. C. H. and Ng, C. W. W. (2015a). Flume investigation of landslide granular debris and water runup mechanisms. *Géotechnique Letters* **5**, No. 1, 28–32.

Choi, C. E., Goodwin, G., Ng, C. W. W., Chu, H. K., Kwan, J. S. H. and Pun, W. K. (2016b). Coarse granular flow interaction with slit-structures. *Géotechnique Letters* **6**, No. 4, 1–8.

Choi, C. E., Liu, H, and Ng, C. W. W. (2018). Impact mechanisms of granular flow against curved barriers. *Géotechnique Letters* **7**, No. 4, 330–338.

Choi, C. E., Ng, C. W. W., Au-Yeung, S. C. H. and Goodwin, G. (2015b). Froude scaling of landslide debris in flume modelling. *Landslides* **12**, No. 6, 1197–1206.

Choi, Y. J. (2010). A Study on Downstream Process of Debris Flow Mobilized from Landslides, Master's Degree, Kangwon National University, 37–44.

Chou, H. T., Cheung, Y. L. and Zhang, S. C. (2007). Calibration of infrasound monitoring system and acoustic characteristics of debris-flow movement by field studies, Debris-flow Hazards Mitigation, Mechanics, Prediction, and Assessment, eds. C. Chenglung and J. Major, Millpress, Rotterdam, 571–580.

Faug, T. (2015). Depth-averaged analytic solutions for free-surface granular flows impacting rigid walls down inclines. *Physical Review E.* **92**, No. 6, 062310.

Faug, T., Chanut, B., Naaim, M. and Perrin, B. (2008a). Avalanches overflowing a dam, dead zone, granular bore and run-out shortening. *Annals of Glaciology* **49**, 77–82.

Faug, T., Naaim, M. and Naaim-Bouvet, F. (2004). An equation for spreading length, center of mass and maximum run-out shortenings of dense avalanche flows by vertical obstacles. *Cold Regions Science and Technology* **39**, No. 2, 141–151.

Faug, T., Naaim, M., Bertrand, D., Lachamp, P. and Naaim-Bouvet, F. (2003). Varying dam height to shorten the run-out of dense avalanche flows,

developing a scaling law from laboratory experiments. *Surveys in Geophysics* **24**, No. 5, 555–568.

Hákonardóttir, K. M., Hogg, A. J., Batey, J. and Wood, A. W. (2003). Flying avalanches. *Geophysical Research Letters* **30**, No. 23, 2191.

Hübl, J., Suda, J., Proske, D., Kaitna, R. and Scheidl, C. (2009). Debris flow impact estimation. In Proceedings of international symposium on water management and hydraulic engineering (ed. C. Popovska), 137–148. Skopje, Macedonia, Ss Cyril and Methodius University.

Iverson, R. M. (2015). Scaling and design of landslide and debris-flow experiments. *Geomorphology* **244**, 9–20.

Iverson, R. M. and Denlinger, R. P. (2001). Flow of variably fluidized granular masses across three-dimensional terrain: 1. Coulomb mixture theory. *Journal of Geophysical Research: Solid Earth*, **106(B1)**, 537–552.

Iverson, R. M. and George, D. L. (2014). A depth-averaged debris-flow model that includes the effects of evolving dilatancy. I. Physical basis. Proceedings of the Royal Society A: Mathematical, Physical and Engineering Sciences, **470**, No. 2170, 20130819. http://doi.org/10.1098/rspa.2013.0819

Iverson, R. M., Logan, M., LaHusen, R. G. and Berti, M. (2010). The perfect debris flow? aggregated results from 28 large-scale experiments. *Journal of Geophysical Research* **115**, F03005, doi:10.1029/2009JF001514

Koo, R. C. H. (2017). Mechanisms of Interaction between Dry Sand Flow and Multiple Rigid Barriers: Flume and Finite-element Modelling. PhD thesis, The Hong Kong University of Science and Technology, Hong Kong.

Koo, R. C. H., Kwan, J. S. H., Ng, C. W. W., Lam, C., Choi, C. E., Song, D. and Pun, W. K. (2017). Velocity attenuation of debris flows and a new momentum-based load model for rigid barriers. *Landslides* **14**, No. 2, 617–629.

Kwan, J. S. H. (2012). Supplementary technical guidance on design of rigid debris-resisting barriers, Technical Note No. TN 2/2012. Hong Kong, SAR China, Geotechnical Engineering Office, Civil Engineering and Development Department, The HKSAR Government.

Kwan, J. S. H., Koo, R. C. H. and Ng, C. W. W. (2015). Landslide mobility analysis for design of multiple debris-resisting barriers. *Canadian Geotechnical Journal* **52**, No. 9, 1345–1359.

Lo, D. O. K. (2000). Review of natural terrain landslide debris-resisting barrier design. Geotechnical Engineering Office, Hong Kong, SAR, China, 91 p. (GEO report no. 104)

Majeed, U. (2020). Designing multiple rigid barrier system for wide range of geophysical flows. PhD thesis (under preparation), The Hong Kong University of Science and Technology, Hong Kong.

Ng, C. W. W., Choi, C. E., Koo, R. C. H., Goodwin, G. R., Song, D. and Kwan, J. S. H. (2018). Dry granular flow interaction with dual-barrier systems. *Géotechnique* **68**, No. 5, 386–399.

Pudasaini, S. P. and Hutter, K. (2007). Avalanche dynamics, dynamics of rapid flows of dense granular avalanches. New York, NY, USA, Springer.

Remaitre, A, Malet, J.-P., Maquaire, O. and Ancey, C. (2003). Study of a debris-flow event by coupling a geomorphological and a rheological investigation, example of the Faucon stream (Alpes-de-Haute-Provence, France), Debris-Flow Hazards Mitigation, Mechanics, Prediction, and Assessment, eds. Rickenmann and Chen, Millpress, Rotterdam, 375–385.

Sze, E. H. Y. and Lam, H. W. K. (2017). Some Suggested Detailing of Flexible net barriers Traversing a Stream Course for Drainage Purposes, GEO Technical Note TN 3/2017, Geotechnical Engineering Office, Hong Kong, SAR, China.

Takahashi T. (1991). Debris flow. Balkema, Rotterdam,165.

Takahashi T. (2007). Debris flow, Mechanics, Prediction and Countermeasures. Taylor and Francis, Leiden, 448.

Tecca, P., Genevois, R., Deganutti, A. and Armento, M.C. (2007). Numerical modelling of two debris-flows in the Dolomites (Northeastern Italian Alps), Debris-flow Hazards Mitigation, Mechanics, Prediction, and Assessment, eds. Chen, C. L. and Major, J. J., Millpress, Rotterdam, 179–188.

VanDine, D. (1996). Debris flow control structures for forest engineering. Ministry of Forests, British Columbia, VIC, Australia.

Volkwein, A. (2014). Net debris flow barriers, Design and application. Swiss Federal Institute for Forest, Snow and Landscape Research WSL.

White, D. J., Take, W. A. and Bolton, M. D. (2003). Soil deformation measurement using particle image velocimetry (PIV) and photogrammetry. *Géotechnique* **53**, No. 7, 619–631.